HRTEM evidence for the process and mechanism of saponite-to-chlorite conversion through corrensite

TAKASHI MURAKAMI,[1,*] TSUTOMU SATO,[2,†] AND ATSUYUKI INOUE[3]

[1]Mineralogical Institute, University of Tokyo, Bunkyo-ku, Tokyo 113, Japan
[2]Department of Environmental Safety Research, Japan Atomic Energy Research Institute, Tokai, Ibaraki 319-11, Japan
[3]Department of Earth Sciences, Chiba University, Chiba 263, Japan

ABSTRACT

To elucidate the process and mechanism of the prograde conversion of saponite to chlorite through corrensite, the microstructures of a series of chlorite-smectite (C-S) mixed-layer samples from Kamikita, northern Japan were examined by high-resolution transmission electron microscopy using both lattice and structure imaging. Corrensite grows epitaxially as domains of 5–20 nm thick mainly within homogeneous saponite domains, without forming randomly interstratified C-S. Then, chlorite domains grow outside homogeneous corrensite domains without forming randomly interstratified C-S or chlorite-corrensite (C-Co), and finally are predominant. An atomic resolution image suggests that corrensite essentially consists of the 1 M stacking of alternating chloritic and smectitic layers. The structure and occurrence suggest corrensite is mineralogically a unique species. Comparison of the stacking vectors of corrensite along [001] to those of chlorite reveals that the stacking sequence is not inherited during the process from corrensite to chlorite. We rarely observed layer terminations of the hydroxide sheets both in corrensite and chlorite domains, and the layer terminations that do exist can be explained as defects rather than the formation of corrensite or chlorite. Our data strongly suggest that the saponite-to-chlorite conversion series progresses stepwise from saponite to corrensite and from corrensite to chlorite, and that the dominant reaction mechanisms are dissolution and precipitation.

INTRODUCTION

Prograde conversion of smectite to chlorite is one of the most fundamental reactions in diagenesis and low-grade metamorphism of intermediate to mafic volcanic rocks and their volcaniclastic sediments. The conversion is characterized by systematic changes in structure and composition associated with interstratified chlorite-smectite layers (C-S) and corrensite at the intermediate steps of the process; it is in general considered to be temperature sensitive as is smectite illitization. Much research concerns the structural and compositional pathways (e.g., reviews by Reynolds 1988; Inoue 1995). However, the details of the conversion, in particular its structural pathway and mechanism, are incompletely understood and actively debated (Beaufort et al. 1997; Bettison-Varga and Mackinnon 1997).

The saponite-to-chlorite conversion has been characterized both as continuous with a gradual decrease in percent of smectite (%S) (e.g., Chang et al. 1986; Bettison and Schiffman 1988; Bevins et al. 1991) and as discontinuous with a stepwise decrease in %S (e.g., Inoue et al. 1984; Inoue and Utada 1991; Schiffman and Staudigel 1995). Continous conversion suggests the presence of randomly interstratified C-S whereas discon-

tinuous conversion suggests its absence. Corrensite, defined as a regular interstratification of trioctahedral chlorite and trioctahedral smectite or vermiculite (Bailey 1982; Brigatti and Poppi 1984), occurs generally in discontinuous conversion. X-ray diffraction analysis (XRD) alone is not sufficient to distinguish different interstratified C-S. However, high-resolution transmission electron microscopy (HRTEM) has shown a wide variety of the microstructures of interstratified C-S; Bettison-Verga et al. (1991) and Bettison-Varga and Mackinnon (1997) reported major occurrence of randomly interstratified C-S in ophiolitic metabasalts. From the presence of randomly interstratified C-S, Bettison-Varga and Mackinnon (1997) proposed a reaction mechanism of smectite to chlorite similar to that of the biotite to chlorite reaction (Veblen and Ferry 1983). The proposed mechanism suggests a half of the 2:1 layer dissolves during the reaction whereas the other half is preserved. Discrete corrensite and chlorite domains or packets are accompanied by interstratified C-S and chlorite-corrensite (C-Co) (Shau et al. 1990; Shau and Peacor 1992; and Jiang and Peacor 1994a and 1994b). Discrete packets of corrensite and chlorite are dominant where relatively high fluid/rock ratios exist (Shau and Peacor 1992). Shau et al. (1990) suggested interstratified C-Co and corrensite-smectite (Co-S) are more stable than randomly interstratified C-S. Two mechanisms for corrensite formation were proposed (Jiang and Peacor 1994b); solid-state transformation, and dissolution and precipitation (see Altaner and Ylagan 1997). Discrete corrensite and chlorite domains or

*E-mail: murakami@min.s.u-tokyo.ac.jp
†Present address: Division of Global Environmental Science and Engineering, Kanazawa University, Kanazawa, Ishikawa 920-1192, Japan.

packets also occur with or without minor amount of interstratified C-Co (Schiffman and Staudigel 1995; Beaufort et al. 1997). The structure and the stability field of corrensite have also been discussed (Velde 1977; Shau et al. 1990; Meunier et al. 1991; Beaufort and Meunier 1994; Jiang and Peacor 1994a; Beaufort et al. 1997).

Some of the previous HRTEM data are not unambiguous: saponite, corrensite, and chlorite were sometimes distinguished only by periodicities along the c* axis (i.e., 1.0, 2.4, and 1.4 nm, respectively) without accounting for the contrast of TEM images. The present study uses appropriate interpretation of HRTEM images to elucidate the process and mechanism of the reaction of saponite to chlorite through corrensite and to better understand the structure of corrensite and structural relationships between reactant corrensite and product chlorite.

SAMPLES AND EXPERIMENTAL METHODS

Samples are from volcaniclastic rocks thermally metamorphosed by diorite intrusion in the Kamikita area, northern Japan. The mineralogy and geology were described in detail by Inoue and Utada (1991) who concluded that the samples represent a prograde metamorphic sequence. The structural variation in the saponite-to-chlorite conversion showed the Kamikita C-S samples were classified into three groups, 100–80%S, ~50%S, and ~0%S, and that samples with 80–50 or 50–0%S were rarely present (Inoue and Utada 1991). Therefore, we selected clay sized fractions (<1 μm) from the above groups and used XRD to examine their d_{001} spacings (Table 1).

For lattice fringe image observation, the specimens were impregnated in resin and cut by ultramicrotomy to create thin films less than 50 nm in thickness (Lee et al. 1975). This process approximately aligns the c* axes of sheet silicates normal to the electron beam. The thin films were placed onto copper TEM grids, coated lightly with carbon, and examined in JEOL JEM 2000FX and Hitachi HF 2000 microscopes. The lattice fringe images of saponite, corrensite, and chlorite normal to the c* axes near Scherzer defocus were interpreted according to Guthrie and Veblen (1990) assuming the smectitic layer of corrensite is similar to phlogopite in phlogopite-chlorite intergrowth; the 2:1 layers and the hydroxide sheets have thicker and thinner black contrast, respectively, and the interlayers of smectite, white contrast. With higher resolution, the 2:1 layers and/or hydroxide sheets may split into a few black contrasts. Images that did not fit the above interpretation, for instance because of thickness or tilt, were excluded from the further discussion of microstructures. The image interpretation is much easier than that of interstratified illite-smectite (I-S), which requires various techniques (e.g., Guthrie and Veblen 1989; Vali and Hesse 1990; Murakami et al. 1993).

TABLE 1. Basal spacings (nm) of saponite, corrensite, and chlorite

Mineral	Sample no.*	%S	XRD	TEM†
Saponite	18-334	~80	1.66 (EG)‡	1.27–1.34
Corrensite	18-360	~50	3.16 (EG)‡	2.62–2.68
Corrensite	17-438	~40	–	–
Chlorite	16-570	~0	1.43	1.43

* After Inoue and Utada (1991).
† The values determined based on selected area electron diffraction.
‡ Ethelyene glycol impregnated.

For atomic resolution image observation, specimen 18-360 was impregnated in resin, pushed between two glass slides, sliced and polished mechanically, and thinned to electron transparency by Ar ion milling. The c* axes of corrensite grains were approximately normal to the electron beam by this process (Ferrow and Roots 1989). The specimen was coated slightly with carbon and examined in a JEOL JEM 2010 microscope with a point resolution of 0.2 nm (Cs = 0.5 mm). Atomic resolution images of corrensite were recorded at a magnification of 400 000–600 000×; TEM negatives were exposed less and developed longer than in the standard process to minimize electron damage. The TEM negatives were digitized and processed to remove noise and the image of amorphous material by rotational filtering (NCEM package of Kilaas and Siddnei implemented within Digital Micrograph V. 2.5, Gatan Ltd.). Simulated images calculated using MacTempas software (Total Resolution Co.) were compared to the filtered images to provide atomic information of the corrensite structure. A similar method was employed by Banfield and Murakami (1998). The crystal structure of corrensite for the simulation was based on that of ferroan clinochlore (Rule and Bailey 1987) assuming the corrensite structure consists of alternating chlorite and smectite; for the structure of the smectitic part, the octahedral and tetrahedral sheets were assumed to be the same as those of the ferroan clinochlore, 0.20 Ca per half a unit (Inoue and Utada 1991) was input for the interlayer removing the original hydroxide sheet, and 1.0 nm for the basal spacing was assumed. The structure of chloritic part of corrensite was assumed to be the same as that of the ferroan clinochlore. For comparison, atomic resolution images of chlorite of sample 16-570 were obtained and processed by a similar method to that for corrensite.

RESULTS

Basal spacing of chlorite (Table 1) did not vary between XRD and TEM as expected. If the d_{001} spacing of the chloritic layer of corrensite is the same as that of chlorite, the d_{001} spacing of the smectitic layer of corrensite is 1.73 nm with ethylene glycol, which is larger than that of glycolated saponite (sample 18-334, Table 1). On the other hand, the d_{001} spacing of the smectitic layer of corrensite was 1.19–1.25 nm under high vacuum of TEM, which was similar to 1.21 nm of saponite (sample 18-334) determined by XRD in a few minutes after heated at 150 °C for 2 hours. Although the d_{001} spacing of the smectitic layer of corrensite collapsed to be about 1.0 nm after long exposure to electron beam, that of saponite remained to be 1.2–1.3 nm.

Sample 18-334 consisted of saponite domains of 5–30 nm thick and, with less amount, of corrensite domains of 5–20 nm thick (Fig. 1a). The d_{001} spacings of saponite varied from 1.2 to 1.35 nm, and completely collapsed saponite layers (~1.0 nm) were rarely observed (Fig. 1b). The saponite domains change their thickness within domains and, thus, have edge dislocations (e.g., arrows in Fig. 1b).

The 2:1 layers, hydroxide sheets and the interlayers of corrensite were clearly imaged, and thus, corrensite was easily distinguished from saponite. Corrensite was observed within homogeneous saponite domains (e.g., the area between the ar-
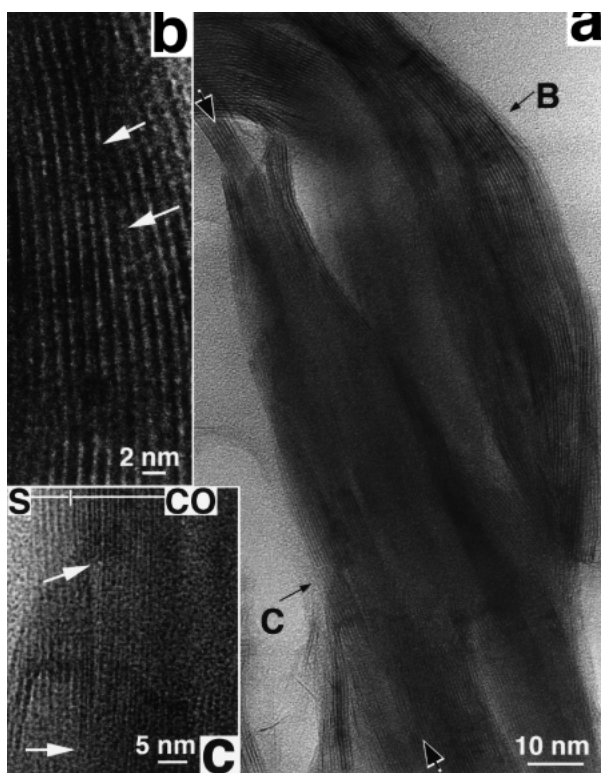
FIGURE 1. Lattice fringe image of saponite and corrensite of sample 18-334. **(a)** Lower magnification showing the microstructural relationship between saponite and corrensite. A corrensite domain of 7.5–18 nm thick in a saponite domain is indicated by the arrows with white rims. **(b)** Higher magnification of smectite near the area indicated by the arrow with B in Figure 1a. Arrows indicate examples of layer terminations. **(c)** Higher magnification of the area indicated by the arrow with C in Figure 1a. S represents a saponite domain and CO a corrensite domain. Arrows indicate layer terminations of corrensite.

FIGURE 2. Rotationally filtered lattice fringe image of corrensite growing in a saponite domain of sample 18-334. **(a)** Image near the area indicated by the arrow with C in Figure 1a, and **(b)** image several tens of nanometers distant from **a**. Figure 2b is arranged so that one can trace the corrensite layers in Figure 2a. The continuity of the corrensite layer is obvious, with a length of this corrensite domain normal to the c* axis of about 350 nm. S represents a saponite domain, and CO a corrensite domain. Corrensite is easily distinguished by black and white contrast; T' represents a 2:1 layer, B a hydroxide sheet, and I an interlayer of the smectitic layer (not labeled for all the layers). The white arrow indicates the termination of a hydroxide sheet; the corrensite layer ends as two 2:1 layers (i.e., two saponite layers) at the bottom of Figure 2a. Pairs of white lines show lattice fringes across those normal to the c* axis. Note they are not in the same direction area by area and even in one layer. The pair of white lines in the saponite domain in Figure 2a indicates that the saponite and corrensite share at least two crystallographic axes in common.

rows with white rims in Fig. 1a) and with much less amount, outside saponite domains. This indicates corrensite grew mainly within saponite domains. Edge dislocations or layer terminations were observed in corrensite domains (arrows in Fig. 1c) and always occurred as disappearance of a set of two 2:1 layers and one hydroxide sheet, i.e., one corrensite layer. The corrensite domain of 7.5–18 nm thick layers (arrows with white rims in Fig. 1a) extends as long as 350 nm, without transformation into saponite layers in the middle of the domain.

Lattice fringe images of two areas (Fig. 2), several tens of nanometers distant from one another, in a corrensite domain within a saponite domain, demonstrate the continuity of the corrensite layers; one can trace the corrensite layers of 350 nm in length although the two corrensite layers at the left of the corrensite domain in Figure 2a terminate and consequently are not seen in Figure 2b. The corrensite and saponite domains have a common c* axis (Fig. 2a). The lattice fringes with a periodicity of about 0.46 nm of the corrensite domain, which is represented by the pairs of white lines in Figures 2a and 2b, vary their directions area by area and even in one layer. The cross fringes in the saponite domains, as seen faintly in the left and

bottom in Figure 2a, are parallel to those of the nearest corrensite layers. Thus, the corrensite present in saponite has almost the same crystallographic axes as those of the host saponite.

Possible layer-by-layer change from saponite to corrensite in a single layer was rarely observed; one example is shown by the white arrow in Figure 2a, which indicates the termination of a hydroxide sheet. The combination of two 2:1 layers and one hydroxide sheet at the top in the right of Figure 2a ends up with that of two 2:1 layers at the bottom. We did not observe randomly interstratified C-S of R0 type in sample 18-334.

FIGURE 3. Lattice fringe image of corrensite in sample 18-360 **(a)** and its selected area electron diffraction **(b)**. The arrow indicates a layer termination of corrensite that has reverse contrast of Scherzer defocus image. The 00*l* diffraction spots occur regularly. **(c)** Lattice fringe image of chlorite (CH) growing outside corrensite domains (CO).

Domains of up to few tens of nanometers thick corrensite were dominant in sample 18-360 (Fig. 3a). Corrensite layers were regularly stacked normal to the c* axis generally, and edge dislocations were sometimes found as layer terminations of single corrensite layers (arrow in Fig. 3a). The SAED patterns of most corrensite domains revealed regular 00*l* diffraction spots (Fig. 3b), indicating a smectitic layer alternates with a chloritic layer regularly. Chlorite domains, although very small in amount, were observed outside homogeneous corrensite domains (Fig. 3c). Chlorite domains were not observed inside corrensite domains; the two types of domains were always found separately. Thus, the occurrence of chlorite domains is different from that of corrensite domains in saponite.

The observed [110] image (Fig. 4a) gives information on the atomic arrangements of the corrensite structure and is compared to the simulated image (Fig. 4b). Pairs of the tetrahedral chains parallel to [110] give spots of black contrast, the hydroxide sheets and the octahedral sheets, lines of black contrast, and the interlayers of the smectitic layers, lines of white contrast (Fig. 4b). The smectitic part is shown by OTITO (O, octahedral sheet; T, tetrahedral sheet; and I, interlayer) in Figure 4b and the chloritic part by OTBTO (B, hydroxide sheet), which are directly compared to the observed image in Figure 4a.

Chlorite polytypes can be identified by the shifts of the spots of black contrast in the tetrahedral sheets across the octahedral

FIGURE 4. Rotationally filtered [110] image of corrensite in sample 18-360 **(a)** and its simulated image **(b)**. The simulated image was made based on the crystal structure of ferroan clinochlore (Rule and Bailey 1987) with a thickness of 5 nm and defocus of –42 nm (Scherzer defocus). The index is assigned assuming also the crystal structure of the clinochlore. See text for the assumptions for the corrensite structure. A thin, white line in Figure 4a is a stacking vector from a pair of tetrahedral cations to another across an octahedral sheet along [001], and a thin, black line, that across an interlayer or hydroxide sheet (e.g., Spinnler et al. 1984). T = tetrahedral sheet; O = octahedral sheet; I = interlayer; and B = hydroxide sheet. Note the smectitic part collapses to about 1 nm (d_{001} spacing) at high magnification (×600 000 for direct observation).

and hydroxide sheets (Spinnler et al. 1984; Bailey 1988). Such shifts are shown in Figure 4a, where the stacking vectors (or offsets) across the octahedral sheets are indicated by thin, white lines, and those across the interlayers or hydroxide sheets by thin, black lines. Spinnler et al. (1984) introduced notations

for the stacking vectors to distinguish a chlorite polytype from another. The stacking vector across the octahedral sheet is denoted by T, and that across the hydroxide sheet by B, and $-$, 0, and $+$ are used as subscripts when the stacking vector is shifted to the left, straight, and to the right, respectively (Spinnler et al. 1984). For instance, the stacking vectors of IIb-6 chlorite are represented by T_0B_+ when viewed down [100], T_+B_0 down [110], and T_-B_+ down [1$\bar{1}$0].

If we apply the notations to corrensite and even to the smectitic part, the stacking vectors of corrensite may be denoted by $T_+B_0T_+B_0$ (Fig. 4a). The stacking vector across the interlayer of the smectitic part, B_0, is consistent with that of trioctahedral mica such as saponite. Polytype of the corrensite was not identified because images of the other zone axes were not obtained. Note the stacking sequence of simulated corrensite (Fig. 4b) is different ($T_+B_+T_+B_+$) because the structure was simply derived from that of IIbb chlorite (Rule and Bailey 1987). Although we had a few structure images of corrensite because of serious beam damage, an atomic resolution image like one

FIGURE 5. [110] lattice fringe image (**a**) and rotationally filtered [100] structure image (**b**) of chlorite in sample 16-570. The black arrows and white bars in the left and right of Figure 5a indicate the 2:1 layers and hydroxide sheets of chlorite, respectively. The hydroxide sheet with a thick arrow in the middle of Figure 5a disappears completely in the left. The white lines in Figure 5b indicate stacking vectors across octahedral sheets, and black lines those across hydroxide sheets. The left and bottom corner demonstrates the corresponding structure of chlorite (Rule and Bailey 1987). Pairs of the tetrahedral chains parallel to [100] give spots of black contrast and the hydroxide sheets and the octahedral sheets, lines of black contrast. Our simulation revealed +20 nm defocus image gives completely reverse contrast of Scherzer defocus image. The image of Figure 5b was taken at +20 nm defocus and processed to have reverse contrast.

in the left of Figure 4a was not observed to spread all over a 7.5–18 nm thick grain even before long exposure to electron. This suggests the crystallographic orientations of neighboring layers are slightly different from one another, resulted partly from the collapse of the smectitic parts due to electron damage at high magnification (400 000–600 000×), and/or that most part of domains is simply damaged.

Sample 17-438 (~40%S) consisted of corrensite and chlorite domains. We observed only an increase in amount of chlorite domains in sample 17-438 compared to sample 18-360 (~50%S). Chlorite domains grow outside corrensite domains as in sample 18-360 (Fig. 3). Thus, the decrease in %S in sample 17-438 simply resulted from the increase in chlorite and decrease in corrensite. Interstratified C-Co was not observed.

Sample 16-570 (~0%S) contained well-crystallized grains (15–50 nm thick) of chlorite which were usually observed as aggregates of several packets with the c* axis in common. A very small amount of saponite domains was also found outside the chlorite grains. Chlorite is observed as alternates of thin, dark fringes (hydroxide sheets, white bars in Fig. 5a) and thick, dark fringes (2:1 layers, black arrows in Fig. 5a). The hydroxide sheet with a thick arrow in the middle of Figure 5a is not always present between the neighboring two 2:1 layers; it disappears completely in the left and repeats presence and absence within the two 2:1 layers of 80 nm long. The complete disappearance of the hydroxide sheet in the left of Figure 5a forms an apparent sequence of one corrensite layer. However, the occurrence of such apparent corrensite layers does not mean the substantial interstratification of C-Co or C-S. Indeed, distinct interstratified C-Co was not observed in sample 16-570. The [100] atomic resolution image (Fig. 5b) shows the stacking vectors across the octahedral sheets (white lines in Fig. 5b) and hydroxide sheets (black lines in Fig. 5b); the stacking sequence of the chlorite may be denoted by $T_0B_0T_0B_-T_0B_0T_0B_-$ $T_0B_0T_0B_0T_0B_+T_0$ from the left to the right in Figure 5b according to Spinnler et al. (1984). We cannot identify a polytype from Figure 5b.

DISCUSSION

Process and mechanism of saponite to chlorite reaction

The process of the saponite-to-chlorite conversion can be summarized: corrensite grows as a domain mainly within a homogeneous saponite domain without forming randomly interstratified C-S or Co-S. This process continues until the corrensite content in C-S mineral is up to 40%, which corresponds to 80% S assuming the interstratification between smectite and chlorite as the end-members. No C-S mineral with 40–100% corrensite (80–50% S) is formed, and corrensite alone is present in the middle of the process. Then, chlorite domains grow outside homogeneous corrensite domains without forming randomly interstratified C-S or C-Co until the corrensite content is down to 80% (40% S). No interstratified C-S or C-Co mineral with 80–0% corrensite (40–0% smectite) is formed, and finally the reaction is completed when chlorite alone is present. The increase in the number of smectitic layers with the progress in the reaction is qualitatively consistent between the XRD and TEM data.

Suquet et al. (1977) and Sato (1992) discussed the relationships between layer charges and basal spacings of trioctahedral

smectites with ethylene glycol solvation; they showed the basal spacings decrease with increase in layer charge if the interlayers are occupied by a single kind of a cation. The interlayers consist mostly of Ca both for the original saponite (sample 18-334) and the smectitic layer of corrensite (sample 18-360) (Inoue and Utada 1991). Therefore, the apparent increase in the basal spacing from the saponite to the smectitic layer of corrensite (1.66 to 1.73 nm) indicates that the smectitic layer of corrensite has a lower charge than that of the precursor saponite, and thus, their compositions of the 2:1 layers are different. This suggests the structural and compositional properties of the tetrahedral layers in saponite are not inherited intactly to those of the smectitic layers in corrensite during the prograde conversion of saponite to corrensite. The lower charge of the smectitic layer of corrensite agrees with the conclusion by Schiffman and Staudigel (1995) that corrensite is chemically a 50:50 mixture of chlorite and low-charge trioctahedral smectite. The lower-charge of the smectitic layers in corrensite than that of the precursor smectite should be compared to the higher-charge of the smectitic layers in rectorite and other R1 I-S discussed by Dong et al. (1997) based on the calculation by Jiang et al. (1990).

Solid-state transformation is well defined for smectite to illite reaction mechanisms by Altaner and Ylagan (1997) who follow the definition used by Veblen (1992) and Baronnet (1992). Solid-state transformation is sometimes referred to as a "layer-by-layer transformation," and typically also involves fluids (Altaner and Ylagan 1997). By atomic-resolution TEM, Kogure and Murakami (1996) and Banfield and Murakami (1998) observed solid-state transformations of biotite to vermiculite and chlorite to vermiculite, respectively, in detail. These observations suggest we should observe the layer termination of a hydroxide sheet and/or transformation from a 2:1 layer to hydroxide sheet if there would be solid-state transformation in the saponite to corrensite reaction. Although we did observe the layer terminations of hydroxide sheets (white arrow in Fig. 2a), the number of the layer terminations was very small, and we did not find any transformation from a 2:1 layer to hydroxide sheet. In addition, we did not observe isolated corrensite with one or two layers in a saponite domain that could indicate the early stage of the solid-state transformation. Thus, the edge dislocation occurring as the layer termination of hydroxide sheets in corrensite domains does not indicate that solid-state transformation is a dominant formation mechanism of corrensite. Instead, corrensite simply grows on or within saponite having almost the same crystallographic axes in common as shown by the epitaxial relationship between saponite and corrensite in Figure 2a. A similar growth process of chlorite in biotite was pointed out by Barronet (1992). He suggested the chlorite forms by epitaxial growth onto (001) of biotite rather than by a solid-state transformation because of the difference in stacking sequence between the two although chlorite grows in a biotite grain sharing b* and c* axes in common in the biotite chloritization.

A comparison of the stacking sequence of corrensite to that of chlorite can give information on the reaction of corrensite to chlorite (Baronnet 1992). The stacking vectors across the octahedral sheets in the 2:1 layers are the same between corrensite and chlorite; T_+ when viewed down [110] for corrensite (Fig.

4a) and T_0 down [100] for chlorite (Fig. 5b). This is not inconsistent with solid-state transformation according to Baronnet (1992). However, in addition to the occurrence of chlorite mentioned above, the difference in the stacking vectors across the interlayers or hydroxide sheets between corrensite and chlorite suggests that solid-state transformation is not operative. The stacking vectors across the interlayers of the smectitic layers in corrensite are normal to the layers (i.e., B_0) viewed down [110], which is characteristic of the mica structure, and those across the hydroxide sheets of the chloritic layers are also represented as B_0. This indicates the stacking vectors across the hydroxide sheets of the chlorite down [100] should have the same signal (B_+, B_-, or B_0) at least every other vector if the stacking vectors of chlorite are inherited from those of corrensite. However, the [100] image of chlorite reveals the stacking vectors across the hydroxide sheets are essentially disordered, i.e., $B_0B_-B_0B_-B_0B_0B_+$ (Fig. 5b). Thus, evidence for the inheritance of stacking from corrensite is lacking.

Although we observed the layer terminations of the hydroxide sheets in chlorite domains (Fig. 5a), the layer terminations should be explained only as defects but not as the formation of interstratified C-S or C-Co as mentioned above for the corrensite formation.

The TEM observation and our interpretation of the TEM images strongly show that a saponite-to-chlorite conversion series progresses stepwise from saponite to corrensite and from corrensite to chlorite, and that the dominant reaction mechanisms are dissolution and precipitation. The solid-state transformation could occur but played little role in the reactions. Although the mechanisms are the same between the saponite-to-corrensite and corrensite-to-chlorite reactions, the different occurrences of corrensite and chlorite, within a host domain (Fig. 2a) and outside a host domain (Fig. 3c), respectively, suggest the free energy change of the saponite-to-corrensite reaction is smaller than that of the corrensite-to-chlorite reactions.

Bettison-Varga and Mackinnon (1997) described dissolution and precipitation similarly for the mechanism of the smectite to chlorite reaction. However, the dissolution mechanism proposed in the present study is different from that by Bettison-Varga and Mackinnon; the former requires entire dissolution of the 2:1 layer of saponite, whereas the latter only a half dissolution and the preservation of the tetrahedral sheet of the other half, which should be rather called solid-state or interlayer-by-interlayer transformation (Altaner and Ylagan 1997). The difference in the proposed mechanisms may be due to genetical differences in specimens such as original rock compositions, fluid/rock ratios, etc.; Bettison-Varga and Mackinnon found randomly interstratified C-S in the groundmass of ophiolitic basalts whereas we did not in the samples from the replacements of groundmass and primary mafic phenocrysts.

Corrensite and interstratified chlorite-smectite

The comparison of the observed [110] image to the simulated one confirms that the corrensite structure consists of alternating chloritic and smectitic structures along [001]. In spite of the limited area of the atomic resolution image, the stacking vectors in Figure 4a suggest corrensite essentially consists of the 1 *M* stacking of chloritic and smectitic layers. This sug-

gests, in addition to the absence of randomly interstratified C-S or Co-S, and the restriction of the composition (i.e., a lower charge of the smectitic part of corrensite than that of the precursor saponite), corrensite is not merely an R1 C-S mixture, but is a unique mineral species.

For the structure of R1 ordered I-S, two fundamental models are proposed (e.g., Hower 1967; Ahn and Peacor 1986; Jiang et al. 1990); in one, the two tetrahedral sheets of a single 2:1 layer are identical in terms of charge and there are two kinds of layer charges, higher and lower, in the 2:1 layers, that is a non-polar 2:1 layer model (hereafter referred to as model 1). In the other, the two tetrahedral sheets bounding the interlayer are identical and the two tetrahedral sheets of a single 2:1 layer are different, that is a polar 2:1 layer model (hereafter referred to as model 2). Model 2 creates potential for ordering of the alternating illitic and smectitic interlayers but model 1 does not. Model 2 is supported by the facts of, for instance, the presence of particles with the thickness of multiples of 2 nm (Ahn and Peacor 1986), the presence of 2 nm-periodic potential in lattice fringe images (Guthrie and Veblen 1989), and the presence of the symmetrical Al-Si distribution across the interlayer (Altaner et al. 1988; Jakobsen et al. 1995). A corrensite structure analogous to R1 completely ordered I-S of model 2 is proposed (Shau et al. 1990; Meunier et al. 1991). Beaufort and Meunier (1994) proposed a third model for corrensite; the two tetrahedral sheets of a single 2:1 layer are identical and there is one kind of layer charge in the 2:1 layers (hereafter referred to as model 3). Our simulations based on models 2 and 3 did not make any significant difference in structure image. The TEM observation revealed the layer termination of corrensite always occurs as TOT-B-TOT, with the interlayers of the smectitic part at outside and the hydroxide sheet at inside (arrows in Figs. 1c and 3a). Thus, the tetrahedral sheets of the smectitic part are exposed to solution. Sample 18-360, corrensite, has Si:Al of 6.15:1.85 at the tetrahedral sites (Inoue and Utada 1991). If we adopt model 3, the exposed tetrahedral sheets have Si:Al of 3.08:0.93, which is the same as that shown by Beaufort and Meunier (1994). It is not likely that such high-charged tetrahedral sheets are always cleaved. Model 2 explains the present TEM observation better than the others do although more data are required to make a definitive conclusion.

The presence of randomly interstratified C-S, Co-S, or C-Co was already reported even by HRTEM (Shau et al. 1990; Bettison-Verga et al. 1991; Shau and Peacor 1992; Jiang and Peacor 1994a, 1994b; Beaufort et al. 1997; Bettison-Varga and Mackinnon 1997) although some of these studies contained ambiguous lattice-fringe images. These observations could infer some similarity in a reaction process and mechanism between the smectite chloritization and illitization. We did not observe any randomly interstratified C-S, Co-S, or C-Co. The layer terminations of the hydroxides found in both corrensite and chlorite domains are interpreted as defects but not as the formation of interstratified structures. The direct conversions of saponite to corrensite and corrensite to chlorite without forming significant amounts of C-S or C-Co observed in the present study suggest the interstratification is much less stable than corrensite in the conversion reaction from saponite to chlorite. Similar discussion was made by Schiffman and Staudigel (1995) who suggest the absence of randomly interstratified C-S

reflects systematically high, integrated fluid fluxes through rocks. Although it has been long believed that randomly interstratified illite-smectite is usually formed during the smectite to illite reaction (e.g., Inoue 1995), the intensive TEM observation by Dong et al. (1997) revealed that R1 ordered I-S is the only exclusive mixed-layer phase. Dong et al. (1997) also concluded that the continuous change from smectite-rich clays to illite-rich clays is due to changes in the proportions of three discrete phases, smectite, R1 ordered I-S, and illite, but not in proportions within single sequences of layers of individual packets. Their conclusion indicates that the reaction progress of saponite to chlorite is directly analogous to that of smectite to illite as is the reaction mechanism, i.e., dissolution and precipitation.

REFERENCES CITED

Ahn, J.H. and Peacor, D.R. (1986) Transmission electron microscope data for rectorite: implications for the origin and structure of "fundamental particles". Clay and Clay Minerals, 34, 180–186.

Altaner, S.P. and Ylagan, R.F. (1997) Comparison of structural models of mixed-layer illite-smectite and reaction mechanism of smectite illitization. Clays and Clay Minerals, 45, 517–533.

Altaner, S.P., Weiss, C.A. Jr., and Kirkpatrick, R.J. (1988) Evidence from ^{29}Si NMR for the structure of mixed-layer illite/smectite clay minerals. Nature, 331, 699–702.

Bailey, S.W. (1982) Nomenclature for regular interstratifications. American Mineralogist, 67, 394–398.

——(1988) Chlorites: Structures and crystal chemistry. In Mineralogical Society of America Reviews in Mineralogy, 19, 347–398.

Banfield, J.F. and Murakami, T. (1998) Atomic resolution transmission electron microscopy evidence for the mechanism by which chlorite weathers to 1:1 semi-regular chlorite-vermiculite. American Mineralogist, 83, 348–357.

Baronnet, A. (1992) Polytypism and stacking disorder. In Mineralogical Society of America Reviews in Mineralogy, 27, 231–288.

Beaufort, D., Baronnet, A., Lanson, B. and Meunier, A. (1997) Corrensite: A single phase or a mixed-layer phyllosilicate in the saponite-to-chlorite conversion series? A case study of Sancerre-Couy deep drill hole (France). American Mineralogist, 82, 109–124.

Beaufort, D. and Meunier, A. (1994) Saponite, corrensite and chlorite-saponite mixed-layers in the Sancerre-Couy deep drill-hole (France). Clay Minerals, 29, 47–61.

Bettison, L.A. and Schiffman, P. (1988) Compositional and structural variations of phyllosilicates from the Point Sal ophiolite, California. American Mineralogist, 73, 62–76.

Bettison-Verga, L. and Mackinnon, I.D.R. (1977) The role of the randomly mixed-layered chlorite/smectite in the transformation of smectite to chlorite. Clays and Clay Minerals, 45, 506–516.

Bettison-Verga, L., Mackinnon, I.D.R., and Schiffman, P. (1991) Integrated TEM, XRD, and electron microprobe investigation of mixed-layered chlorite-smectite from the Point Sal ophiolite, California. Journal of Metamorphic Geology, 9, 697–710.

Bevins, R.E., Robinson, D., and Rowbotham, G. (1991) Compositional variations in mafic phyllosilicates from regional low-grade metabasites and application of the chlorite geothermometer. Journal of Metamorphic Geology, 9, 711–721.

Brigatti, M.F. and Poppi, L. (1984) Crystal chemistry of corrensite: A review. Clays and Clay Minerals, 32, 391–399.

Chang, H.K., Mackenzie, F.T., and Schoonmaker, J. (1986) Comparisons between the diagenesis of dioctahedral and trioctahedral smectite, Brazilian offshore basins. Clays and Clay Minerals, 34, 407–423.

Dong, H., Peacor, D.R., and Freed, R.L. (1997) Phase relations among smectite, R1 illite-smectite, and illite. American Mineralogist, 82, 379–391.

Ferrow, E.A. and Roots, M. (1989) A preparation technique for TEM specimens; applications to synthetic Mg-chlorite. European Journal of Mineralogy, 1, 815–819.

Guthrie, G.D. Jr. and Veblen, D.R. (1989) High-resolution transmission electron

microscopy of mixed-layer illite/smectite: Computer simulations. Clays and Clay Minerals, 37, 1–11.

——(1990) Interpreting one-dimensional high-resolution transmission electron micrographs of sheet silicates by computer simulation. American Mineralogist, 75, 276–288.

Hower, J. (1967) Order of mixed-layering in illite/montmorillonite. In S.W. Bailey, Ed., Clays and clay minerals, Proceedings of 15th National Conference, Pittsburgh, Pennsylvania, 1966, p. 63–74. Pergamon Press, New York.

Inoue, A. (1995) Formation of clay minerals in hydrothermal environments. In B. Velde, Ed., Origin and mineralogy of clays, p. 268–329. Springer, Berlin.

Inoue, A. and Utada, M. (1991) Smectite-to-chlorite transformation in thermally metamorphosed volcanoclastic rocks in the Kamikita area, Northern Honshu, Japan. American Mineralogist, 76, 628–640.

Inoue, A., Utada, M., Nagata, H., and Watanabe, T. (1984) Conversion of trioctahedral smectite to interstratified chlorite/smectite in Pliocene acidic pyroclastic sediments of the Ohyu district, Akita Prefecture, Japan. Clay Science, 6, 103–116.

Jakobsen, H.J., Nielsen, N.C., and Lindgreen, H. (1995) Sequences of charged sheets in rectorite. American Mineralogist, 80, 247–252.

Jiang, W.-T. and Peacor, D.R. (1994a) Prograde transitions of corrensite and chlorite in low-grade pelitic rocks from the Gaspé Peninsula, Quebec. Clays and Clay Minerals, 42, 497–517.

——(1994b) Formation of corrensite, chlorite and chlorite-mica stacks by replacement of detrital biotite in low-grade pelitic rocks. Journal of Metamorphic Geology, 12, 867–884.

Jiang, W.-T., Peacor, D.R., Merriman, R.J., and Roberts, B. (1990) Transmission and analytical electron microscopic study of mixed-layer illite/smectite formed as an apparent replacement product of diagenetic illite, Clays and Clay Minerals, 38, 449–468.

Kogure, T. and Murakami, T. (1996) Direct identification of biotite/vermiculite layers in hydrobiotite using high-resolution TEM. Mineralogical Journal, 18, 131–137.

Lee, S.Y., Jackson, M.L., and Brown, J.L. (1975) Micaceous occlusions in kaolinite observed by ultramicrotomy and high resolution electron-microscopy. Clays and Clay Minerals, 23, 125–129.

Meunier, A., Inoue, A., and Beaufort, D. (1991) Chemiographic analysis of trioctahedral smectite-to-chlorite conversion series from the Ohyu caldera, Japan. Clays and Clay Minerals, 39, 409–415.

Murakami, T., Sato, T., and Watanabe, T. (1993) Microstructure of interstratified illite-smectite at 123K: A new Method for HRTEM examination. American Mineralogist, 78, 465–468.

Reynolds, R.C. Jr. (1988) Mixed layer chlorite minerals. In Mineralogical Society of America Reviews in Mineralogy, 19, 601–629.

Rule, A.C. and Bailey, S.W. (1987) Refinement of the crystal structure of a monoclinic ferroan clinochlore. Clays and Clay Minerals, 35, 129–138.

Sato, T. (1992) Crystallochemical study of expandable clay minerals—Relationship between expansion, dehydration, and rehydration and crystallochemical factors. 96 p. Ph. D. dissertation, Waseda University, Tokyo, Japan.

Shau, Y.-H. and Peacor, D.R. (1992) Phyllosilicates in hydrothermally altered basalts from DSDP Hole 504B, Leg 83—A TEM and AEM study. Contributions to Mineralogy and Petrology, 112, 119–133.

Shau, Y.-H., Peacor, D.R., and Essene, E.J. (1990) Corrensite and mixed-layer chlorite-corrensite in metabasalts from northern Taiwan: TEM/AEM, EMPA, XRD and optical studies. Contributions to Mineralogy and Petrology, 105, 123–142.

Schiffman, P. and Staudigel, H. (1995): The smectite to chlorite transition in a fossil seamount hydrothermal system: the Basement Complex of La Palma, Canary Islands. Journal of Metamorphic Geology, 13, 487–498.

Spinnler, G.E., Self, P.G., Iijima, S., and Buseck, P.R. (1984): Stacking disorder in clinochlore chlorite. American Mineralogist, 69, 252–263.

Suquet, H., Iiyama, J. T., Kodama, H., and Pezerat, H. (1977) Synthesis and swelling porperties of saponites with increasing layer charge. Clays and Clay Minerals, 25, 231–242.

Vali, H. and Hesse, R. (1990) Alkylammonium ion treatment of clay minerals in ultrathin section: A new method for HRTEM examination of expandable layers. American Mineralogist, 75, 1443–1446.

Veblen, D.R. (1992) Electron microscopy applied to nonstoichiometry, polysomatism, and replacement reactions in minerals. In Mineralogical Society of America Reviews in Mineralogy, 27, 181–229.

Veblen, D.R. and Ferry, J.M. (1983) A TEM study of the biotite-chlorite reaction and comparison with petrologic observations. American Mineralogist, 68, 1160–1168.

Velde, B. (1977) Clays and clay minerals in natural and synthetic systems, 218 p. Elsevier, Amsterdam.